Low-temperature proton spin–lattice relaxation maxima of lanthanum hydrides doped with paramagnetic rare earth ions

2004 J. Phys.: Condens. Matter 16 6147

(http://iopscience.iop.org/0953-8984/16/34/014)

INSTITUTE OF PHYSICS PUBLISHING JOURNAL OF PHYSICS: CONDENSED MATTER

J. Phys.: Condens. Matter **16** (2004) 6147–6158 PII: S0953-8984(04)80920-2

Low-temperature proton spin–lattice relaxation maxima of lanthanum hydrides doped with paramagnetic rare earth ions

S Leyer[1], R G Barnes[2], C Buschhaus[1], G Fischer[1], B Pilawa[1], B Pongs[1], A Tinner[1] and E Dormann[1]

[1] Physikalisches Institut, Universität Karlsruhe (TH), D-76128 Karlsruhe, Germany
[2] Department of Physics and Ames Laboratory, USDOE, Iowa State University, Ames, IA 50011, USA

Received 17 May 2004
Published 13 August 2004
Online at stacks.iop.org/JPhysCM/16/6147
doi:10.1088/0953-8984/16/34/014

Abstract

The low-temperature proton spin–lattice relaxation is analysed for lanthanum hydrides LaH_x intentionally doped with Gd or Ce. These paramagnetic impurities were also characterized by static magnetic susceptibility and electron spin resonance measurements. A quantitative description of the proton relaxation rate maxima, as well as of the electron spin relaxation data, is presented. These analyses indicate that the density of states at the rare earth site disappears only for $x \gtrsim 2.9$.

1. Introduction

The comparably fast reversible switching of thin films from optical transparency to reflectivity via the hydrogen content [1, 2] has revived interest in the metal–insulator (MI) and order–disorder (OD) transitions of rare earth hydrides [3–6]. In an attempt to extend proton–spin relaxation measurements of nominally pure LaH_x hydrides ($2 \leqslant x \leqslant 3$) to lower temperatures, a low-temperature relaxation maximum was observed in the 20–40 K range [7]. For further comparison, respective results are reproduced in figure 1. A relaxation rate maximum is observed that increases roughly like $\omega_0^{-2/3}$ with decreasing Larmor frequency. The proposed explanation of the spin–lattice relaxation maximum by a motion induced dipolar contribution contrasted with the rather smooth increase of the linewidth for decreasing temperature (figure 3 of [7]), however. As an alternative, and in line with earlier relaxation studies of nonmagnetic La or Y hydrides that were intentionally doped with paramagnetic rare earth ions [6], one of the present authors (RGB) suggested proton spin diffusion to accidental, relaxing, electronic impurity moments as an explanation of the low-temperature rate maximum. Indeed, a laser

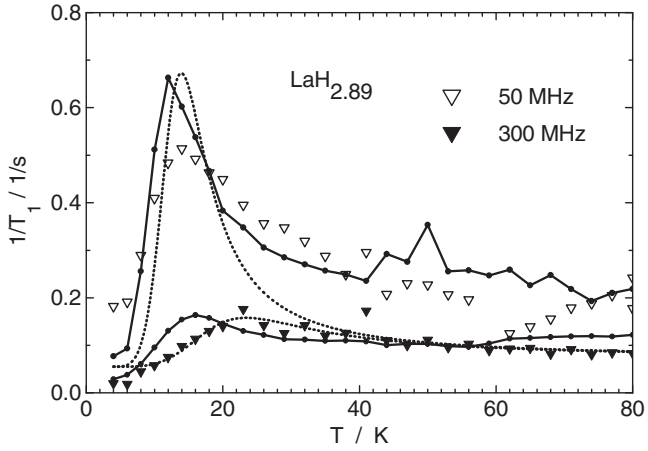

Figure 1. Influence of the Larmor frequency on the low-temperature proton spin–lattice relaxation maximum of nominally pure $LaH_{2.89}$. The broken curves show the comparison with a BPP-like relaxation mechanism proposed in [7]. The two solid curves connecting data points show the superposition of the experimentally derived contributions of 10 ppm Ce and 5 ppm Gd to proton relaxation for the two Larmor frequencies.

source mass spectrometric analysis of the lanthanum used allowed for <20 ppm Ce, <10 ppm Gd and[3] 33 ppm Yb as the most relevant impurities.

Therefore, in this communication, we report low-temperature proton–spin relaxation results for three lanthanum hydrides intentionally doped with a substantially larger concentration of rare earth ions, i.e. metallic $LaH_{2.26}$:100 ppm Gd and 'nonmetallic' $LaH_{2.87}$:300 ppm Gd and $LaH_{2.89}$:2700 ppm Ce. From the thus magnified influence of these impurities on proton relaxation we can conclude that such impurities can cause the low-temperature relaxation maxima reported in [7] and by other authors [8]. Our paper is organized as follows. In section 2 we describe the relevant experimental details and present the respective results. These are analysed and discussed in section 3, while section 4 collects the conclusions.

2. Experimental details and results

The powder samples $LaH_{2.26}$:100 ppm Gd, $LaH_{2.87}$:300 ppm Gd and $LaH_{2.89}$:2700 ppm Ce were prepared at the Materials Preparation Center of Ames Laboratory, Iowa State University from highest purity lanthanum. A hardened steel mortar and pestle were used to break up the alloy hydride button into fragments. Then an agate mortar and pestle were used to grind the fragments down to approximately 40 μm size. The samples were those used in earlier nuclear magnetic resonance (NMR) studies [6, 9].

The powder samples were sealed in quartz ampoules of about 6 mm diameter for the NMR measurements. For proton NMR at $\nu_0 = 300$ MHz, a Bruker MSL 300 spectrometer with a 70 kG superconducting magnet, for $\nu_0 = 200$ MHz a Bruker CXP 200 spectrometer with a 47 kG magnet, and for $\nu_0 = 80$ and 53 MHz a Bruker CXP 200 spectrometer and electromagnet, were used with Oxford Instruments gas-flow variable temperature cryostats. For derivation of the spin–lattice relaxation time T_1, the inversion-recovery spin–echo sequence with phase cycling was adopted (pulse lengths 3.2 and 1.6 μs). Single-exponential recoveries were observed. The results are shown in figures 2–4 for the two magnetic impurities Gd and Ce. The linewidth was verified via Fourier transformation of the second half of the echo. Line splittings in the high-temperature phase are observed as was reported before [3, 10].

The static magnetic properties were derived with a Quantum Design MPMS SQUID magnetometer, with the powder sample surrounded by a helium atmosphere during

[3] Chemical analysis by Materials Preparation Center, Ames Laboratory, Iowa State University.

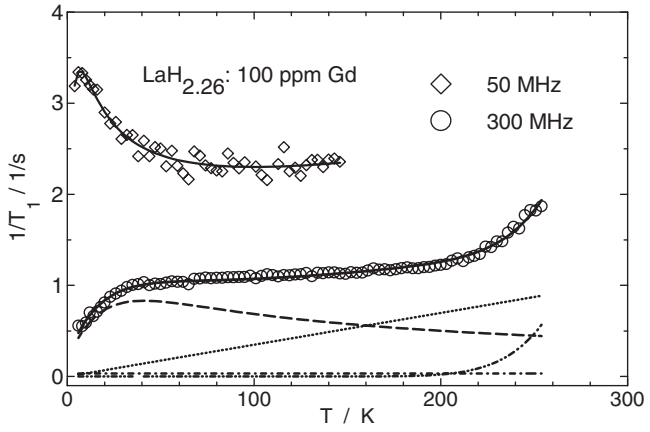

Figure 2. Proton spin–lattice relaxation rate of $LaH_{2.26}$:100 ppm Gd for two Larmor frequencies ($\nu_0 = 50$, 300 MHz) versus temperature. The solid curve fits are explained in the text. For illustration, in the 300 MHz data the distinct contributions of Gd impurities, conduction electrons, oxidation or magnetically ordered surface defects, and proton hopping motion are indicated as dashed, dotted, dot–dashed, and dot–dot–dashed curves, respectively (for parameters see table 1).

the measurements. Unfortunately, the oxidation of the powder grain's surface during these measurements could not reliably be prevented. Various field strengths between 0.1 and 50 kOe were applied. The raw data of the field- and temperature-dependent magnetic moment were corrected for a small content of a magnetically ordered impurity phase, estimated to be about 300 μg Fe per 1 g of the doped lanthanum hydride samples, not inconsistent with the sample preparation procedure (table 1). To emphasize saturation effects the moment divided by field data were extrapolated to $1/H \rightarrow 0$. The corrected data for $LaH_{2.89}$:2700 ppm Ce are presented in figure 5 as the weight related magnetic susceptibility χ_ρ and as the product $(\chi_m - \chi_{dia})T$, related to one mole of the rare earth ion Ce. A Curie–Weiss fit between 8 and 235 K (broken curve) gives $\mu_{eff} = 1.69\ \mu_B$, $\theta = -0.8$ K and $\chi_{dia} = -2.27 \times 10^{-7}$ emu g^{-1}, whereas the solid curve fit for the whole temperature range, ignoring the transition at about 240 K, gives $\mu_{eff} = 2.12\ \mu_B$, $\theta = -7.3$ K and $\chi_{dia} = -2.57 \times 10^{-7}$ emu g^{-1}. A better way to analyse the data is to look at the product $(\chi_m - \chi_{dia})T$. This representation reveals the deviation of the diamagnetic part of the total magnetic susceptibility from the calculated value $\chi_{dia} = -20 \times 10^{-6}$ emu mol$_{RE}^{-1}$ via the negative slope, and the Curie constant and effective moment via the T-versus-zero extrapolated value. For the high-temperature range $T > 250$ K, the derived effective moment $\mu_{eff} = 2.54\ \mu_B$ corresponds to the Ce^{3+} free ion moment. The reduced moments of 1.56 μ_B for the low-temperature range (8–50 K) and of 1.92 μ_B for the 50–235 K range reveal substantial crystal field effects. For the Gd-doped samples $LaH_{2.26}$:100 ppm Gd and $LaH_{2.87}$:300 ppm Gd, on the other hand, correction for the magnetic impurities was less successful, yielding, for example, an effective moment of $\mu_{eff} = 16.3\ \mu_B$ above 40 K, by about a factor of two larger than the expected free ion moment, for the latter sample.

In order also to unravel the temperature dependence of the electronic spin flip rate of the paramagnetic rare earth ions Gd^{3+} and Ce^{3+}, respectively, in the low-temperature phase of the lanthanum hydrides LaH_x, the temperature dependence of the electron spin resonance (ESR) line width of the powder samples was determined at 9.5 GHz with a Bruker ESP-300E spectrometer using a helium gas flow cryostat for temperature control. For metallic $LaH_{2.26}$:100 ppm Gd a linear increase of the Gd^{3+} ESR linewidth with temperature of $\Delta B_{PP}/\Delta T = 10 \pm 10$ G K^{-1} was derived. The results for $LaH_{2.87}$:300 ppm Gd are shown in figure 6. The central line with $g \approx 1.98$ can clearly be distinguished in the absorption derivative ESR powder spectrum. Its intensity decreases in an essentially Curie-like manner with T, with minor offset caused by the broadening of the overlapping neighbouring lines

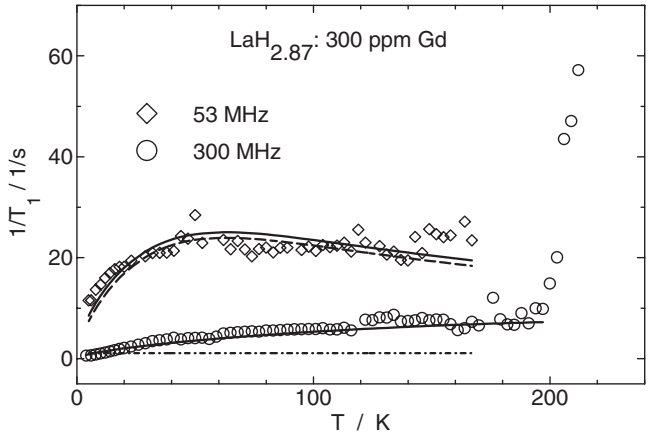

Figure 3. Proton spin–lattice relaxation rate of $LaH_{2.87}$:300 ppm Gd for two Larmor frequencies ($\nu_0 = 53$, 300 MHz) versus temperature. The solid curve fit is explained in the text. For illustration, in the 53 MHz data the distinct contribution of Gd impurities and 'defects' (see figure 2) are indicated as dashed and dot–dashed curves, respectively (for parameters see table 1).

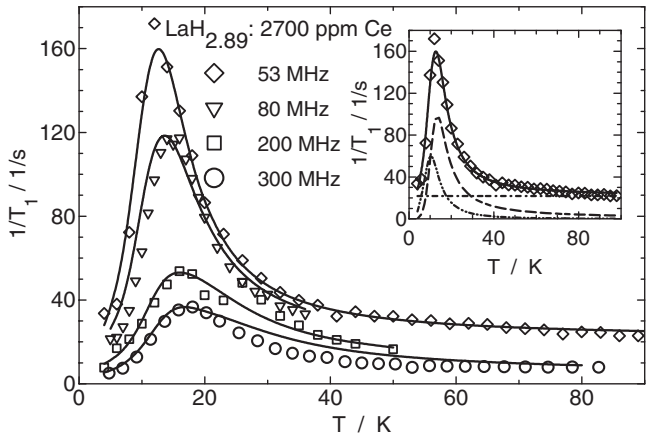

Figure 4. Proton spin–lattice relaxation rate of $LaH_{2.89}$:2700 ppm Ce for four Larmor frequencies ($\nu_0 = 53$, 80, 200 and 300 MHz) versus temperature. The solid curve fit is explained in the text. For the 53 MHz data, the inset also shows the distinct contribution of Ce impurities via the Orbach process (equation (6*d*), LF) or according to equation (6*b*) (HF) and oxidation or magnetically ordered surface defects as dashed, dot–dot–dashed and dot–dashed curves, respectively (for parameters see table 1).

(solid curve in inset to figure 6; right-hand part). The linewidth increase with temperature is reduced in comparison to the metallic sample by more than one order of magnitude to $\Delta B_{PP}/\Delta T \approx 0.4$ G K^{-1}. For $LaH_{2.89}$:2700 ppm Ce, the central line group (CL; $g_x = 2.08$, $g_y = 2.05$, $g_z = 2.008$) may originate from oxidized sample surface portions resembling the arrangement in the CeO_2 crystalline phase; its width of $\Delta B_{1/2} \approx 21$–25 G shows no pronounced temperature dependence (figure 7). The high-field (HF) lines ($g_{\mathrm{eff}} < 1.2$) showed in part a dramatic nonlinear line width increase with temperature (up to 100 G K^{-1}) and could not be observed for temperatures above 10 K due to their large width. The ESR parameters of the low-field (LF) signal are plotted as a function of temperature in the left-hand part of figure 7. While the g value ($g \approx 2.98$) remains constant for $T < 20$ K, the linewidth increases with temperature indicative of a thermally activated contribution (see equation (6*d*) below).

3. Discussion

In pure lanthanum hydrides LaH_x, $2 \leqslant x \leqslant 3$, for temperatures above 200 K, proton spin–lattice relaxation is dominated by the influence of hydrogen atom diffusion [6]. This contribution, $(T_{1\mathrm{d}})^{-1}$, is displayed by the dash-double dotted curve in figure 2 for the 300 MHz proton relaxation data. It is evidently of minor importance for the behaviour at $T < 200$ K investigated here, and is therefore disregarded in the following. For hydrides LaH_x with

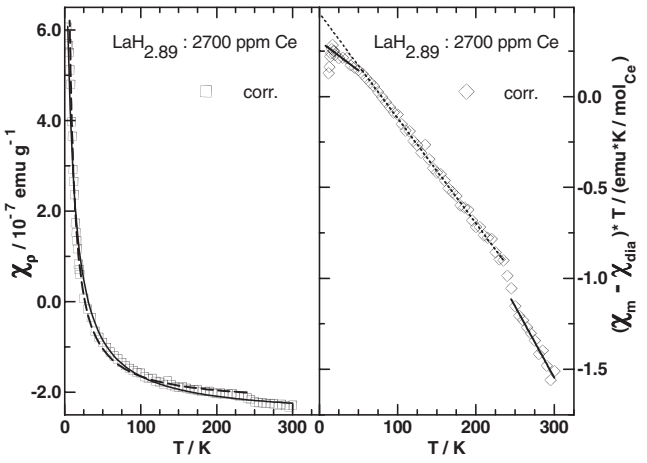

Figure 5. Temperature dependence of the weight related magnetic susceptibility χ_ρ and of the product of mole related, diamagnetism corrected magnetic susceptibility and temperature, i.e., $(\chi_m - \chi_{dia})T$, for Ce-doped sample $LaH_{2.89}$:2700 ppm Ce. The solid and broken curve fits are explained in the text.

Table 1. Fit parameters for proton relaxation rates in rare earth doped LaH_x samples.

Composition	$LaH_{2.26}$:100 ppm Gd	$LaH_{2.87}$:300 ppm Gd	$LaH_{2.89}$:2700 ppm Ce	
Fe impurity	539 μg Fe/g	321 μg Fe/g	235 μg Fe/g	
Korringa slope	3.5×10^{-3} (s K)$^{-1}$	—	—	
RE-contribution			(HF)	(LF)
p (equation (4))	0.54	0.63	0.56	1.0
$N\rho$	1.2×10^5 s$^{-1.54}$	9.4×10^6 s$^{-1.63}$	5.8×10^6 s$^{-1.56}$	6.5×10^{10} s^{-2}
a	4.4×10^7 s^{-1} K^{-1}	5.3×10^6 s^{-1} K^{-1}	—	—
A	—	—	3.7×10^3 s^{-1} K$^{-4.9}$	—
n	—	—	4.9	—
α	—	—	—	1.4×10^{10} s^{-1}
Δ/k_B (equation (6d))	—	—	—	50 K
Impurity contribution[a]				
R	4.1 s^{-1}	4.1 s^{-1}	24.4 s^{-1}	
τ_c	5.0×10^{-9} s	5.0×10^{-9} s	1.1×10^{-9} s	
Proton hopping contribution[b]				
r	9.3×10^4 s^{-1}			
W/k_B	3.05×10^3 K			

[a] $(1/T_1)_{imp} = R(1 + \omega_0^2\tau_c^2)^{-1}$.
[b] $(1/T_1)_{ph} = r \exp(-W/k_BT)$.

hydrogen concentration below the critical concentration for the metal–insulator transition $x_c \approx 2.86$ [5], a Korringa-like additional proton spin–lattice relaxation rate proportional to temperature, $(T_{1e})^{-1}$, is induced by the interaction with the conduction electrons, that can be clearly discerned in the low-temperature range $T < 150$ K [6, 7]. For the metallic $LaH_{2.26}$:100 ppm Gd sample, this Korringa-like contribution is visualized in figure 2 by the dotted line (table 1). The relaxation rate induced by paramagnetic impurities like Gd or Ce is superimposed on these intrinsic rates and may predominate by far, at least in the low-temperature range. Again, two ranges have to be distinguished. In the high-temperature range, $T > 200$ K, the hydrogen atoms are able to diffuse into the neighbourhood of the paramagnetic localized impurities. This contribution has been analysed in detail in earlier investigations [6, 11]. By contrast, in the low-temperature range, proton–spin diffusion is

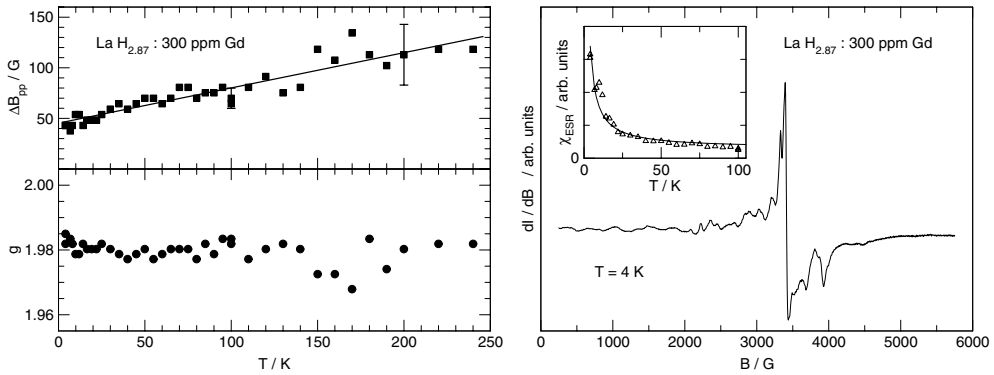

Figure 6. ESR analysis (9.5 GHz) of $LaH_{2.87}$:300 ppm Gd powder sample. The right-hand side shows a typical absorption derivative ESR spectrum and the temperature dependence of the central line intensity as an inset. On the left-hand side, for the central line, the variation of peak-to-peak line width and g-factor are plotted versus temperature. The solid curve fits are explained in the text; see also table 1.

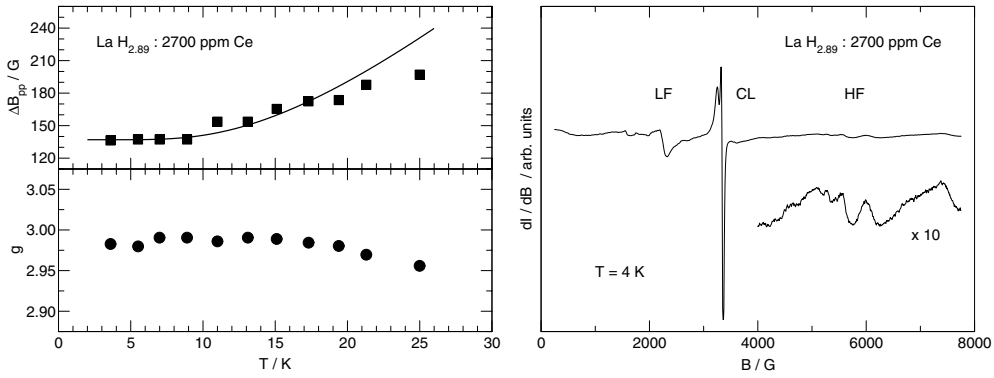

Figure 7. ESR analysis (9.5 GHz) of $LaH_{2.89}$:2700 ppm Ce powder sample. The right-hand side shows a typical absorption derivative ESR spectrum. On the left-hand side, for the low-field line (LF), the variation of peak-to-peak linewidth and g-factor are plotted versus temperature. The solid curve fit is explained in the text; see also table 1.

required to bring the relaxing influence of the magnetic impurities into action, and the bordering cases of fast or slowly relaxing impurities have to be distinguished.

A low-temperature peak in the relaxation rate occurs for $\omega_0\tau_i = 1$, where ω_0 is the proton Larmor frequency, and τ_i is the spin lattice relaxation time of the paramagnetic impurity ion, Gd^{3+} or Ce^{3+}, respectively. This is clearly different from the proton–proton dipolar interaction, where the condition $\omega_0\tau_d = 1$ of the rate maximum requires the thermally activated proton-jump rate τ_d^{-1} to equal ω_0.

We concentrate on the low-temperature range, $T < 200$ K. We emphasize, however, that our measurements show clearly the narrowing of the NMR linewidth for increasing hydrogen hopping rate in the temperature range above 200 K, the occurrence of a structural phase transition at 240 K for $LaH_{2.89}$:2700 ppm Ce, reflected even in the magnetic susceptibility measurements (figure 5), and of two separate proton lines in the high-temperature phase of $LaH_{2.89}$:2700 ppm Ce.

A qualitative inspection of figures 3 and 4 of the 'nonmetallic' hydrides $LaH_{2.87-2.89}$ indicates that the cerium impurities have a greater influence on the relaxation rate at lower temperatures and the gadolinium impurities at higher temperatures. From a quantitative point of view, at about 100 K, 300 ppm of the $4f^7$ ion Gd^{3+} have the same influence as 2700 ppm of the $4f^1$ ion Ce^{3+}. These impurity contents raise the proton spin lattice relaxation rate at 100 K by about a factor of 100 compared to the nominally pure LaH_x compounds of [7] (figures 3 and 4 as against figure 1). Judged from the temperature of the rate maximum in figure 1, the cerium impurities of this nominally pure lanthanum hydride were most efficient for the impurity-induced relaxation rate. The linear dependence of the rate maximum on impurity concentration (equations (2) and (3), below) limits the impurity content of the nominally pure samples to less than 27 ppm Ce or 7.5 ppm Gd (or, for the best fit in figure 1 (solid curve), 5 ppm Gd plus 10 ppm Ce). The qualitative comparison of figures 2 and 3 indicates that the Gd^{3+} induced proton relaxation rate maximum occurs at considerably lower temperature for the metallic $LaH_{2.26}$ sample than for the 'nonmetallic' $LaH_{2.87}$ sample. Evidently, Gd^{3+} spin lattice relaxation is about one order of magnitude faster for $LaH_{2.26}$ than for $LaH_{2.87}$. The maximum rate for the Ce-doped sample decreases with increasing proton Larmor frequency with an $\omega_0^{-0.95}$-frequency dependence (figure 4).

3.1. Modelling of the impurity induced relaxation contribution

The strength of the proton–impurity moment interaction is defined by $\tau^{-1}(r) = Cr^{-6}$, where $\tau^{-1}(r)$ is the relaxation rate that a single proton would have at a distance r from the impurity ion. For powder samples, C is given by [12, 13]

$$C = \tfrac{2}{5}(\gamma_p\gamma_e\hbar)^2 J(J+1)\left[\tau_i/(1+\omega_0^2\tau_i^2) + 7\tau_i/3(1+\omega_e^2\tau_i^2)\right] \tag{1}$$

where γ_e, ω_e, J, and τ_i are the gyromagnetic ratio, Larmor frequency, angular momentum and spin–lattice relaxation time of the paramagnetic ion, and γ_p and ω_0 concern the proton. In the temperature range of interest here, the second term within the square brackets is negligible, since $\omega_e^2\tau_i^2 \gg 1$.

The relative importance of direct relaxation characterized by C and that due to spin diffusion, D_S, is described by the pseudo-potential radius, $\beta = (C/D_S)^{1/4}$, which is the distance from the impurity at which the rate of diffusion to the impurity equals the relaxation rate at the distance from the impurity. A second important parameter in the low-temperature regime is the spin-diffusion barrier radius, b, which is roughly the distance at which the magnetic field due to the impurity ion equals the local nuclear dipolar field at a proton site in the lattice, and within which spin diffusion is inhibited [12]. The relative significance of b and β is expressed by the parameter $\delta = \beta^2/2b^2 = (C/D_S)^{1/2}/2b^2$.

Limiting forms of the relaxation rate, $(T_{1p})^{-1}$, appropriate to the fast and slow spin diffusion regimes, i.e., the weak and strong collision regimes, respectively, are determined by δ. Approximately, $\delta \geqslant 2$, or $\beta \geqslant 2b$, defines the strong collision regime in which

$$(T_{1p})^{-1} = (8\pi/3)NC^{1/4}D_S^{3/4}$$

or

$$(T_{1p})^{-1} = (8\pi/3)NG^{1/4}D_S^{3/4}[\tau_i/(1+\omega_0^2\tau_i^2)]^{1/4} \tag{2}$$

where, for brevity, $G = (2/5)(\gamma_p\gamma_e\hbar)^2 J(J+1)$.

The weak collision regime is defined by $\delta \lesssim 0.3$, or $\beta \lesssim 0.8b$, with

$$(T_{1p})^{-1} = (4\pi/3)NCb^{-3}$$

or

$$(T_{1p})^{-1} = (4\pi/3)NGb^{-3}[\tau_i/(1+\omega_0^2\tau_i^2)]. \tag{3}$$

Since $\tau_i = \omega_0^{-1}$ when $(T_{1p})^{-1}$ reaches its maximum, $(T_{1p})^{-1}_{max}$, it is evident that, in the strong collision case, $(T_{1p})^{-1}_{max} \propto \omega_0^{-1/4}$, and in the weak collision case $(T_{1p})^{-1}_{max} \propto \omega_0^{-1}$. In the classical theory [13], in the intermediate regime, $0.8b \gtrsim \beta \gtrsim 2b$, which spans the transition from $\omega_0^{-1/4}$ to ω_0^{-1} behaviour; $(T_{1p})^{-1}$ depends on Bessel functions of fractional order, $I_m(\delta)$.

An alternative approach [14] to this intermediate regime that avoids the considerable uncertainties in determining the spin-diffusion coefficient D_S and the barrier radius b, which depends on the ion moment, magnetic field strength and temperature, is to express $(T_{1p})^{-1}$ as

$$(T_{1p})^{-1} = N\rho[\tau_i/(1 + \omega_0^2\tau_i^2)]^p \tag{4}$$

with $1/4 < p < 1$, and with ρ used as an adjustable parameter in fitting the temperature- and frequency-dependent proton relaxation data. The frequency dependence of $(T_{1p})^{-1}_{max}$ is now given by ω_0^{-p}. The fit of this general form to the proton relaxation rate data depends sensitively on the assumed temperature dependence of any additional relaxation contributions as depicted in figure 2. Therefore, reliable direct information on the static and dynamic properties of Gd- and Ce-electron spin systems is required for the quantitative analysis of proton spin relaxation.

3.2. Statics and dynamics of the Gd- and Ce-electron spins

3.2.1. Gd impurities. As expected, the static magnetic susceptibility of the Gd^{3+} $4f^7$ half-filled shell impurity of $LaH_{2.26}$:100 ppm Gd and $LaH_{2.87}$:300 ppm Gd follows a Curie law with no pronounced temperature-dependent anomalies. This is also evidenced by the temperature dependence of the ESR intensity of the latter sample (figure 6). The ESR intensity of the metallic sample resides at the detection limit of our experimental set-up. Therefore, the linewidth's linear increase $\Delta B_{PP}/\Delta T = 10 \pm 10$ G K^{-1} could only be derived with a large error bar. This slope compares favourably with the experimental results for $Tm_{1-x}Gd_xH_2$ [15]. In the low-temperature limit of this metallic van Vleck system, a bottleneck situation for the relaxation of the Gd electronic spins via the conduction–electron spins to the lattice was observed. Thus the slope of the linear increase of the linewidth increased from 1.1 G K^{-1} for $x = 0.01$, to 4.25 G K^{-1} for $x = 0.005$, and to 7.15 ± 0.1 G K^{-1} for $x = 0.001$. The latter values approach the slope of the metallic $LaH_{2.26}$ sample analysed here. For a Lorentzian line shape, we can estimate the electronic spin flip rate τ_i^{-1} via

$$\tau_i^{-1} = \gamma_e(\Delta B_{PP}(T) - \Delta B_{PP}(0)) \times 3^{1/2}/2. \tag{5}$$

The Gd ESR spectrum of the $LaH_{2.87}$:300 ppm Gd powder sample is broad as well (figure 6), and shows considerable influence of zero-field splitting and crystal fields. In the critical hydrogen concentration range $x \approx x_c$, it is *a priori* not clear if the temperature dependence of the electronic spin flip rate τ_i^{-1} still follows the Korringa law

$$\tau_i^{-1} = aT \tag{6a}$$

with the Korringa slope 'a' proportional to the squared product of 4f-conduction electron exchange integral and conduction electron density of states, as was reported for $x \approx 2.0$ [15], or if a higher power

$$\tau_i^{-1} = AT^n \tag{6b}$$

with $n = 5 \cdots 9$ typical for Kramers ions with crystal field splitting in an insulator, or the temperature dependence typical for the direct relaxation process,

$$\tau_i^{-1} = a' \coth\left(\frac{\hbar\omega}{2k_BT}\right) \tag{6c}$$

is more appropriate [16]. Figure 6 shows the best fit of a linear variation to the temperature dependence of the central line ESR linewidth. The nominally nonmetallic lanthanum hydride

$LaH_{2.87}$ studied here gives for its very low Gd concentration, where no bottleneck of the relaxation is expected, a slope of 0.38 ± 0.05 G K^{-1} that is smaller by a factor of 2.5 than the bottleneck of the metallic dihydride systems. Thus,the spin–lattice relaxation of the Gd^{3+} $4f^7$ electron spins in the weakly metallic or nonmetallic sample $LaH_{2.87}$:300 ppm Gd studied here is indeed very slow.

3.2.2. Ce impurities. Neutron and Raman scattering for CeD_x revealed that the Ce^{3+} $4f^1$ ion has a quartet (Γ_8) ground state and an excited doublet (Γ_7) state located at about 20 meV in the cubic dideuteride for $x \approx 1.95$ [17]. For $1.95 < x < 3$, the Γ_8 ground state of at least some of the Ce sites splits into two doublets, with maximum splitting of about 5 meV (58 K) [17]. For $LaH_{2.89}$:2700 ppm Ce, the static magnetic susceptibility (figure 5) reflects a ground state level splitting by a break in slope of χT at about 50 K, with a low-temperature effective moment (powder average!) of $\mu_{\rm eff} = 1.56\ \mu_{\rm B}$ ($T < 50$ K) and a high-temperature value of $1.92\ \mu_{\rm B}$ (55–235 K). Only at temperatures above 250 K, i.e. above the evident phase change at about 235–250 K, does the effective moment, $\mu_{\rm eff} = 2.54\ \mu_{\rm B}$, agree with the free-ion value of the Ce^{3+}–$^2F_{5/2}$ state ($g = 6/7$, $\mu_{\rm eff} = g\sqrt{J(J+1)}\ \mu_{\rm B} = 2.535\ \mu_{\rm B}$). Thus a complicated temperature and orientation dependence of the electron–spin relaxation times has to be expected, that is not easy to unravel based on a powder sample ESR analysis. Nevertheless, the main ingredients of the proton relaxation contributions are clearly exhibited by the ESR analysis:

(i) There are some Ce sites in $LaH_{2.89}$:2700 ppm Ce that show very fast relaxation (HF lines, figure 7). Their contribution to equation (1) reaches the condition for a proton relaxation rate maximum, $\omega_0\tau_{\rm i} = 1$, already at temperatures below 15 K. The temperature dependence of $\tau_{\rm i}^{-1}$ can be approximated by equation (6*b*) with an exponent $n = 5$.

(ii) In the case that the $g \approx 2$ oxide centres (CL in figure 7) exist at all in the NMR samples, they have very slow spin–lattice relaxation. Even for the smallest proton Larmor frequency ($\nu_0 = 53$ MHz), the condition for a rate maximum $\omega_0\tau_{\rm i} = 1$ is not reached by far. Thus, these centres will at best give rise to a ω_0^{-2} contribution in equation (1).

(iii) The Ce^{3+} sites that are reflected by the LF–ESR lines (figure 7) have a surrounding that gives rise to a crystal-field splitting of the Ce^{3+} lowest quartet into two doublets. Hence, the temperature dependence of the LF–ESR linewidth (figure 7) indicates a resonant Raman or Orbach relaxation process [16]

$$\tau_{\rm i}^{-1} = \alpha/(\exp(\Delta/kT) - 1) \tag{6d}$$

with an activation energy of $\Delta/k_{\rm B} = 50$ K, in clear agreement with the static magnetic susceptibility data. These sites evidently contribute to the low-temperature proton relaxation rate maxima.

3.3. Proton relaxation rates

Based on this additional independent information about the magnetic properties and dynamics of the rare earth impurities Gd^{3+} and Ce^{3+} in LaH_x hydrides, a quantitative description of the proton spin–lattice relaxation rates can be given that is shown as solid curves in figures 2–4.

3.3.1. Gd-doped lanthanum hydrides. As discussed above, the maximum of the proton spin–lattice relaxation rate occurs at that temperature $T_{\rm max}$, for a proton Larmor frequency ν_0, for which the condition $2\pi\nu_0\tau_{\rm i} = 1$ is fulfilled, equation (1). For a frequency-independent

relaxation process like the Korringa relaxation (equation (6*a*)), the respective broadening of the 'homogeneous' Gd ESR linewidth must then amount to (equation (5))

$$\Delta B_{PP}(T_{\max}) - \Delta B_{PP}(0) = 2(3^{-1/2})\nu_0(\gamma_e/2\pi)^{-1}. \tag{7}$$

For Gd^{3+} ($g_e \approx 2$) this increase amounts to about 22 G for $\nu_0 = 53$ MHz or 124 G for $\nu_0 = 300$ MHz. For Gd^{3+} in the metallic hydride $LaH_{2.26}$:100 ppm Gd, the Korringa relaxation of the Gd electron spin guarantees these relaxation rates (or linewidth increases) already in the temperature range below 20 K, as indicated by the slope $\Delta B_{PP}/\Delta T = 10 \pm 10$ G K^{-1} derived above. The best fit of figure 2 yields $\Delta B_{PP}/\Delta T = 2.9$ G K^{-1}. This explains the low-temperature proton relaxation maxima at about 7 K (50 MHz) and 43 K (300 MHz) in figure 2 (or in [8]). On the other hand, for the lanthanum hydrides with hydrogen concentration $x \geqslant x_c \approx 2.86$, it is questionable if a Korringa-like contribution exists at all at low temperatures. The ESR linewidth increase of 0.35 G K^{-1} (figure 6) can be described as well by equation (6*a*) as by (6*c*). However, the experimental data plotted in figure 6 indicate unequivocally that the central ESR line of Gd^{3+} in $LaH_{2.87}$:300 ppm Gd exhibits the former increase (22 G) in the 50–100 K range, thus causing the 53 MHz proton relaxation rate maximum in figure 3 with equation (6*a*), i.e., the Korringa relaxation rate of the Gd impurity. The latter value (124 G), required for a $\nu_0 = 300$ MHz rate-maximum, is not reached even at room temperature, however. Thus, we conclude that the small and weakly temperature-dependent Korringa-like spin–lattice relaxation rate (equation (6*a*)) of the Gd^{3+}-impurity electron spin in the barely metallic lanthanum hydrides explains correctly the flat temperature and pronounced frequency dependence of the proton spin–lattice relaxation rate plotted in figure 3 for $LaH_{2.87}$:300 ppm Gd. On the other hand, the faster Korringa relaxation of Gd electron spins and of the protons explains easily the low-temperature rate maxima and the overall linear increase, respectively, of the proton spin lattice relaxation rate in the metallic $LaH_{2.26}$:100 ppm Gd (figure 2). The parameters of the solid curve fits in figures 2, 3 and 6 are collected in table 1. For completeness, an impurity contribution is included, which is required only for the Ce-doped sample, but is irrelevant for the Gd-doped samples (see figure 2). It takes care of the influence of the magnetically ordered surface impurities and eventual rare earth oxides.

3.3.2. Ce-doped lanthanum hydride. The ESR spectrum of this sample pointed to three different contributions of the magnetic impurities to proton relaxation. The LF ESR line, with an Orbach relaxation process, must be affiliated with the low-temperature proton relaxation rate maximum in figure 4. Indeed, according to equation (5), this rate maximum is predicted for $\nu_0 = 50$ MHz at $T_{\max} = 12$ K according to the ESR line-broadening data of figure 7, i.e., a broadening by 14.8 G, in close agreement with the proton NMR result. Figure 4 proves by the approximate ω_0^{-1} frequency dependence of this proton relaxation rate maximum, which corresponds to the behaviour according to equations (1) and (3), that these Ce impurity sites, that can use the fast Orbach relaxation process, are actually relaxing the protons only by a fast diffusion weak collision mechanism (i.e., $p = 1.0$ in equation (4)).

On the other hand, the plateau-like contribution to proton relaxation at T above 40 K evidently corresponds to Ce sites with slow electron spin relaxation. The strong frequency dependence of the proton relaxation plateau height identifies again a fast diffusion but weak collision mechanism (according to equations (1) and (3)). As in the case of the Gd-doped samples, this contribution may be caused by magnetically ordered surface impurities or by eventual rare earth oxides. The solid curve fit in figure 4 includes therefore an impurity contribution adopting a temperature-independent τ_c-value (table 1).

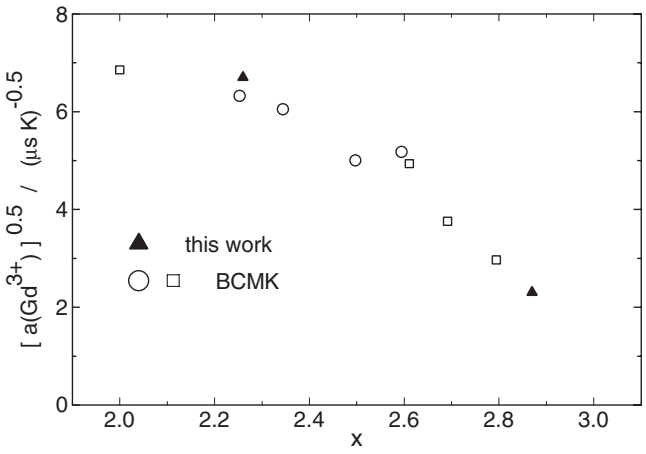

Figure 8. Relaxation data for Gd^{3+} electron spins in LaH_x versus hydrogen content x, given as the square root of the Korringa-like temperature-dependent slope, proportional to the conduction electron density of states. Open symbols: low- or high-temperature data (squares or circles, respectively) reported by BCMK [11]. Full triangles: this work.

The solid curve fit in figure 4 also takes into account the HF ESR lines of the $LaH_{2.89}$:2700 ppm Ce sample with very fast electron spin relaxation (adopting equation (6*b*), with $n \approx 5$). According to the fit result, $p = 0.56$ (equation (4)), these sites influence proton spin relaxation intermediately, between the limiting cases of weak or strong collision, and fast or slow diffusion, respectively. This contribution influences (and makes more pronounced) the low-temperature wing of the proton relaxation rate maxima, and gives a relaxation strength that is comparable to that of the Ce sites with an Orbach relaxation process.

In summary, ESR, SQUID and proton relaxation data can be described quantitatively, with minor deviations only for the high-temperature wing of the Ce impurity induced proton relaxation maximum at the highest measuring frequency.

4. Concluding remarks

The temperature and frequency dependence of proton spin lattice relaxation in Gd-doped and Ce-doped lanthanum hydrides has been measured and analysed quantitatively (figures 2–4). The solid curve shown in figure 1 proves that the low-temperature proton relaxation maxima of the nominally pure lanthanum hydrides reported in [7] can be explained by the contribution of about 5 ppm Gd and 10 ppm Ce paramagnetic impurities of these samples. For Gd^{3+}, we analysed the contribution of the rare earth moment to proton relaxation in the metallic hydride $LaH_{2.26}$:100 ppm Gd and in $LaH_{2.87}$:300 ppm Gd, which is at the bordering concentration $x \approx 2.86$ [5] for the metal–nonmetal transition. Our analysis indicates that the relaxation of the Gd^{3+} electron spin can be better described by a Korringa-like frequency-independent, T-linear contribution (equation (6*a*)) than the direct spin–phonon relaxation process (equation (6*c*)) that gives also a T-linear, but frequency-dependent contribution. This enables us to add the $(a)^{1/2}$ data of the $LaH_{2.87}$:300 ppm Gd sample to the plot of $a^{1/2}$ versus H concentration x derived in [11]; see figure 8. In addition, the data point for the $LaH_{2.26}$-sample shows that this work provides independent confirmation of the earlier measurement which was made at high temperature. This figure represents the variation of the conduction electron density of states at the rare earth site of LaH_x with x, the interpretation relying only on the x-independence of the

4f-spin conduction electron spin exchange integral. The $x = 2.87$-data point supports clearly the suggestion [11] that the conduction electron density of states at the rare earth site in LaH_x hydrides, determined for the low temperature phase, is lost above $x \approx 2.9$ and below $x = 3$.

The situation for Ce^{3+} impurities is much more complicated, in accordance with the occurrence of different structural sites in $LaH_{2.89}$:2700 ppm Ce (local surroundings) and with their complicated crystal field level scheme. However, by combination with an ESR analysis, the different contributions could be separated, one of them being an Orbach relaxation process of the rare earth moment, indicating a level splitting by $\Delta / k_B = 50$ K, responsible for the low-temperature relaxation maximum of the protons. In spite of the complicated orientation- and site-dependent Ce^{3+} electron spin dynamics, the Ce^{3+} contribution to proton relaxation could be parameterized quantitatively.

Acknowledgments

We thank H Wipf and G Majer for discussions and the Deutsche Forschungsgemeinschaft for financial support. Ames Laboratory is operated for the US Department of Energy by Iowa State University under Contract W-7405-Eng-82. This work was supported by the Director for Energy Research, Office of Basic Energy Sciences.

References

[1] Huiberts J N, Griessen R, Rector J H, Wijngaarden R J, Dekker J P, de Groot D G and Koeman N J 1996 *Nature* **380** 231
[2] van Gogh A T M, Nagengast D G, Kooij E S, Koeman N J, Rector J H, Griessen R, Flipse C F J and Smeets R J J G A M 2001 *Phys. Rev.* B **63** 195105
[3] Schreiber D L and Cotts R M 1963 *Phys. Rev.* B **131** 1118
[4] Barnes R G, Chang C T, Belhoul M, Torgeson D R, Beaudry B J and Peterson D T 1991 *J. Less-Common Met.* **172–174** 411
[5] Shinar J, Dehner B, Barnes R G and Beaudry B J 1990 *Phys. Rev. Lett.* **64** 563
[6] Barnes R G 1997 *Topics in Applied Physics* vol 73, ed H Wipf (Heidelberg: Springer) p 93
[7] Leyer S, Weizenecker J and Dormann E 2000 *J. Phys.: Condens. Matter* **12** 6927
[8] Zogal O J, Vuorimäki A H and Ylinen E E 2000 *Phil. Mag.* A **80** 2549
[9] Barnes R G, Beaudry B J, Creel R B, Torgeson D R and de Groot D G 1980 *Solid State Commun.* **36** 105
[10] Barnes R G, Beaudry B J, Torgeson D R, Chang C T and Creel R B 1997 *J. Alloys Compounds* **253/254** 445
[11] Barnes R G, Chang C T, Majer G and Kaess U 2003 *J. Alloys Compounds* **356/357** 137
[12] Phua T T, Beaudry B J, Peterson D T, Torgeson D R, Barnes R G, Belhoul M, Styles G A and Seymour E F W 1983 *Phys. Rev.* B **28** 6227
[13] Rohrschach H E Jr 1964 *Physica* **30** 38
[14] Fukushima E and Uehling E A 1968 *Phys. Rev.* **173** 366
[15] Shaltiel D, Burger J P, Daou J N, Vajda P and Grayevsky A 1991 *Phys. Rev.* B **43** 6022
[16] Abragam A and Bleaney B 1970 *Electron Paramagnetic Resonance of Transition Ions* (Oxford: Clarendon) p 60 f
[17] Arons R R 1991 *Landolt–Börnstein New Series* Group III, vol 19d1 (Berlin: Springer) p 347